Analysis of Fluctuation-Induced Firing in the Presence of Inhibition

Chris Christodoulou[1, a, b], Trevor G Clarkson[b], Guido Bugmann[c] and John G Taylor[d]
[a]*Dept of Computer Science, Birkbeck College, University of London, Malet Street, London WC1E 7HX, UK*
[b]*Dept of Electronic Engineering,* [d]*Dept of Mathematics, King's College London, University of London, Strand, London, WC2R 2LS, UK*
[3]*School of Computing, University of Plymouth, Drake Circus, Plymouth PL4 8AA, UK*

Abstract. This paper examines the computational role of inhibition as it moves towards balancing concurrent excitation using the biologically-inspired Temporal Noisy-Leaky Integrator (TNLI) neuron model. The TNLI incorporates hyperpolarising inhibition with negative current pulses of controlled shapes and it also separates dendritic from somatic integration. The function of inhibition is investigated by examining its effect on the transfer function of the neuron and on the membrane potential. Increasing inhibition leads to greater membrane potential fluctuations as well as greater amplitude variations for a given level of mean input current. This added variance leads to decreasing the slope of the neuron's transfer function (mean input current *vs* mean output frequency), effectively reducing the gain of the input/output sigmoid; inhibition can therefore be used as a means of controlling the gain of the transfer function. Moreover, we demonstrate that in the case of balanced excitation and inhibition (where the neuron is totally driven by membrane potential fluctuations), the neuron's firing rate can be controlled by the level of mean input frequency.

1. Introduction

Nerve cells influence each other by *excitation* and *inhibition*. Many excitatory and inhibitory inputs are received by a cell (*synaptic convergence*) which in turn supplies many others (*synaptic divergence*). Depending on the relation of the equilibrium potential for the conductance to the membrane potential level, there exist two types of effect of the inhibitory synapses: *shunting*, and *hyperpolarising* inhibition (Shepherd & Koch, 1990). The process whereby a cell adds together all the incoming signals that excite and inhibit is known as *synaptic integration*. Synaptic integration is and is nonlinear and complex (Rall, 1964) and depends on relation of the membrane potential to the excitatory and inhibitory equilibrium potentials. Theoretical models (Shepherd & Koch, 1990) show that synaptic inhibition on concurrent synaptic excitation has a nonlinear character which becomes more linear the more hyperpolarising the inhibition and enables it to be used in operations equivalent to addition and subtraction in the dendrites. By contrast, for purely shunting inhibition, the effect is most nonlinear and it is believed to be able to perform operations computationally equivalent to multiplication and division in its interactions with excitatory inputs (Küpfmüller & Jenik, 1961).

In this paper we study the effect of concurrent excitation and inhibition on the membrane potential and the transfer function of the neuron, as the level of inhibition increases. More interestingly, in the case of balanced inhibition and excitation, we examine whether and how the neuron's firing rate can be controlled. The case of balanced excitation and inhibition has recently attracted considerable interest after it has been demonstrated that it causes chaotic behaviour in the state of neurons (Van Vreeswijk and Sompolinsky, 1996; 1998) and has been used in theoretical models to examine irregular neural firing (Shadlen and Newsome, 1994; 1998; Feng & Brown, 1998).

2. Neuron Model Used: The Temporal Noisy-Leaky Integrator

For this study we used the TNLI neuron model (Christodoulou *et al.*, 1992; 1994), which is a simple, biologically inspired and hardware realisable computational model. Fig. 1 shows an analogue hardware outline of the TNLI using a pRAM (probabilistic RAM, Clarkson *et al*., 1992) at each input and a Hodgkin and Huxley (1952) equivalent circuit for a leaky cell membrane (implementational details of the TNLI digital hardware realisation can be found in Christodoulou *et al.*, 1992 and its theoretical analysis in Christodoulou *et al.*, 1994). The 1-pRAMs in the TNLI model the stochastic and spontaneous neurotransmitter release by the synapses of real neurons. The 0-pRAMs shown in the model are used in the simulations to produce random spike input trains from other neurons of controlled mean input frequency, according to their probability $\alpha = p$. The postsynaptic response (PSR) generators (Fig. 1), model the effects of dendritic propagation of the postsynaptic potentials and in particular their *temporal summation*, i.e., the translation of the frequency of incoming spikes into a magnitude of a net postsynaptic potential (Nicholls *et al.*, 1992). The presynaptic transmitter release creates an ion-specific conductance change in the postsynaptic neuron which in the TNLI we approximate with an inward or outward current flow model (Christodoulou *et al.*, 1994). The separation of dendritic and somatic integration makes the current-based model approximation necessary, because a current input is needed to the leaky integrator circuit following in the model, which is the *active* single-compartment representing the somatic membrane. We have therefore, voltage as output of that circuit, representing

[1] Corresponding author; Email Address: *chris@dcs.bbk.ac.uk*

the somatic membrane potential. For every spike generated by the pRAMs, the PSR generators produce postsynaptic current responses $PSR_{ij}(t)$ (i.e., a postsynaptic response at neuron i caused by an input spike at time t from input neuron j), of controlled shapes, shown in Fig. 1 (at inputs n and $n + m$), which can either be excitatory (Excitatory Postsynaptic Currents, EPSCs) or inhibitory (Inhibitory Postsynaptic Currents, IPSCs). Such EPSCs and IPSCs extended in time, have been used previously in the form of an alpha function (see Walmsley & Stuklis, 1989 and references therein). In the TNLI, these particular ramp shapes chosen for the PSRs are an approximation of alpha functions in the form of linear splines that can easily be implemented in digital hardware.

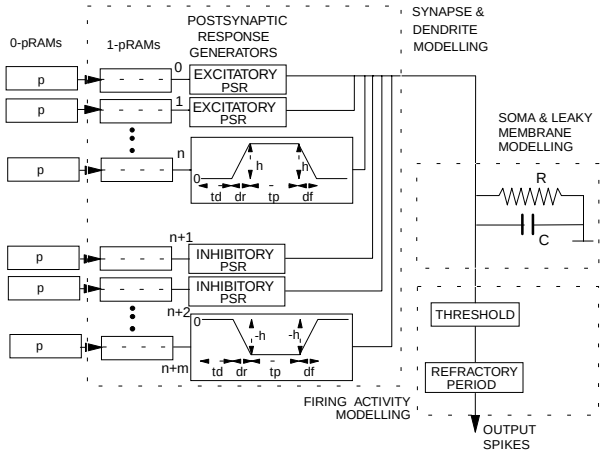

Fig. 1: Analogue hardware outline of the TNLI neuron model. The dotted line boxes indicate the corresponding parts of the real neuron which the TNLI modules are inspired by. At inputs n and $n + m$, the Postsynaptic Current Response shapes utilised are shown (EPSCs and IPSCs respectively) where: $\boldsymbol{t_d}$: Synaptic delay time, $\boldsymbol{t_p}$: Peak Period time, $\boldsymbol{d_r}$: Rise time, $\boldsymbol{d_f}$: Fall time, $\boldsymbol{h}$: Postsynaptic Peak Current.

The EPSCs and IPSCs are then summed spatio-temporally and the total postsynaptic current response is fed into the RC circuit (Fig. 1). The synaptic saturation that occurs in the real neuron during the temporal summation of the postsynaptic potentials (Burke and Rudomin, 1977) is not currently modelled in the TNLI, but it could be easily incorporated by applying the methods used in Bugmann (1992). The capacitance C and the resistance R represent the somatic leaky membrane of real neurons and therefore this circuit models the decay that occurs in the somatic potential of the real neuron due to its membrane leak. The capacitance C and the resistance R are fixed at a suitable value to give the leaky membrane time constant ($\tau = RC$). For simplicity, the TNLI does not differentiate in its leaky integrator circuit between different ionic currents as may occur in the real neuron. If the potential of the capacitor exceeds a constant threshold (V_{th}), then the TNLI neuron fires. It then waits for an absolute refractory period (t_R) and fires again if the membrane potential is above the threshold after the refractory period elapses. Therefore, the maximum firing rate of the TNLI is given by $1/t_R$. In this model the integration of inputs continues during the refractory time, but without having the value of the membrane potential compared with the firing threshold during that time. Depending on the application for which the TNLI is being used, the membrane potential, i.e., the potential of the capacitor, can be completely discharged or *reset* whenever the neuron fires (Christodoulou *et al.*, 1994) (as in as in Lapique (1907) or not reset at all (Christodoulou *et al.*, 1992) as in Bressloff & Taylor (1991) or partially reset (as in Bugmann *et al.*, 1997). For the simulations described in this paper, *no reset* was applied on the somatic potential of the TNLI for an easier observation and analysis of the membrane potential.

3. Computational Function of Inhibition: Methods and Data Used

In the TNLI we only incorporate hyperpolarising inhibition with negative current pulses of controlled shape (IPSCs, Fig. 1), and not shunting inhibition. Such responses are produced by certain PSR generators which are assigned to be inhibitory ones. In practice, this is achieved by programming a negative value for the postsynaptic peak current, h (Fig. 1), in a register. The number of inhibitory PSR generators which corresponds to inhibitory inputs is thus variable. In order to demonstrate the effects of inhibition, we vary this number and observe the change in the relationship between the Mean Input Current in neuron i (I_{M_i}) and the output frequency of the TNLI. I_{M_i} in the TNLI neuron i is given by:

$$I_{M_i} = \sum_{j=0}^{N} f_j \times PSR_{ij}^{*} \qquad \textbf{(1)}$$

where f_j is the mean input spike frequency which in our simulations is the same for each input j and is given by the number of input spikes during time T (total time that the system is left to operate). N is the total number of input lines (or pRAMs). PSR_{ij}^{*} is the time integral of the postsynaptic current (PSR_{ij}) produced by a spike arriving on input line j i.e.,

$$PSR_{ij}^{*} = \int_{0}^{d_r + t_p + d_f} PSR_{ij}(t)\ dt \qquad \textbf{(2)}$$

Results were taken with 100 excitatory PSR generators and 0, 20, 40, 60, 80, 95 and 100 inhibitory ones (denoting the number of excitatory and inhibitory synaptic inputs). The parameter values used for the postsynaptic current

responses (Fig. 1) are: t_d = 5ms, $d_r = d_f$ = 5ms, t_p = 10ms, h = 5pA. For simplicity, the inhibitory currents have an equal but opposite magnitude to the excitatory ones (-5pA). The other TNLI parameters are: t_R = 2ms, R = 166MΩ, V_{th} = 15mV, C = 60pF. The simulation time step used was Δt = 1ms and the system was left to operate for T = 10000ms. The membrane time constant $\tau = RC$ = 10ms lies within the realistic value range. At the TNLI inputs, random spike trains of controlled mean frequency (f_j) were utilised with $f_j = p/\Delta t$, where p is the 0-pRAM probability value. These random spike trains were unaffected by the 1-pRAM action in the current simulations.

4. Results, Analysis and Discussion

While the number of inhibitory inputs was increased, we had to increase f_j, in order to obtain the same I_{M_i}. For instance, the f_j required at the TNLI inputs to give the same I_{M_i} = 100pA, increased from 13.5 Hz to 17Hz, 22.2Hz, 33.5, 70.5 and to 260Hz as the inhibitory PSR generator number (denoting the number of inhibitory synaptic inputs) increased from 0 to 20, 40, 60, 80 and to 95 respectively. The output characteristic for the first six configurations above is shown in Fig. 2, where we also plotted the output frequency values of the balanced case of 100ex/100inh, in which case $I_{M_i} \simeq 0$. In addition, Fig. 2 shows a plot of the excitatory component of I_{M_i} ($I_{M_{i_{ex}}}$) with the output firing frequency for the case of 100 excitatory and 40 inhibitory inputs. As it can be observed (Fig. 2) the TNLI gives a relatively steep sigmoidal nonlinear transfer function (esp. for low inhibition). This is due to the fact that for these simulations the somatic membrane potential is not reset after each spike (Bugmann *et al.*, 1997). The sigmoidal transfer function has a smooth and differentiable behaviour (positive derivative), which enables learning to be achieved using standard methods (Rumelhart *et al.*, 1986). This behaviour seems to be similar to that of the formal neuron (McCulloch & Pitts, 1943), which has a sigmoid transfer function given by: $y = 1/[1 + exp(-\gamma A_i)]$, where γ is a constant that determines the slope of the sigmoid and A_i is given by: $\sum x_j w_{ij}$ where x_j is the *jth* input to the neuron *i* and w_{ij} is the connection weight form neuron *j* to neuron *i*. A_i is equivalent to I_{M_i} in the TNLI (eqn. 1). Fig. 2 demonstrates that the introduction of the inhibition has the same effect as decreasing the value of γ in the sigmoid whereas in formal neurons inhibition only affects A_i. I_{M_i} is also modified when inhibition is introduced; the plot of $I_{M_{i_{ex}}}$ (excitatory component of I_{M_i}) with the output firing frequency for the case of 100 excitatory and 40 inhibitory inputs, shows that the sigmoid (and the threshold) is shifted horizontally toward higher $I_{M_{i_{ex}}}$ values which denotes that higher $I_{M_{i_{ex}}}$ is needed to obtain the same firing rate.

For explaining why the slope of the sigmoid transfer function decreases as the strength of the introduced

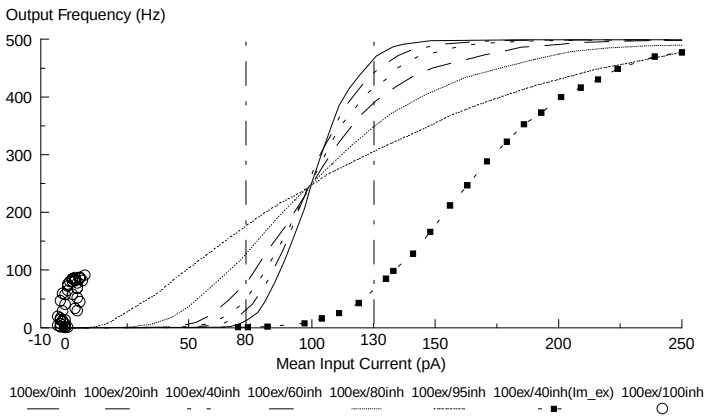

Fig. 2: Transfer functions (TF) of the TNLI (Mean Input Current *vs* firing rate) with different levels of inhibition (see legends/text). TFs saturate at an output frequency of approx. 500Hz (which is equal to $1/t_R$).

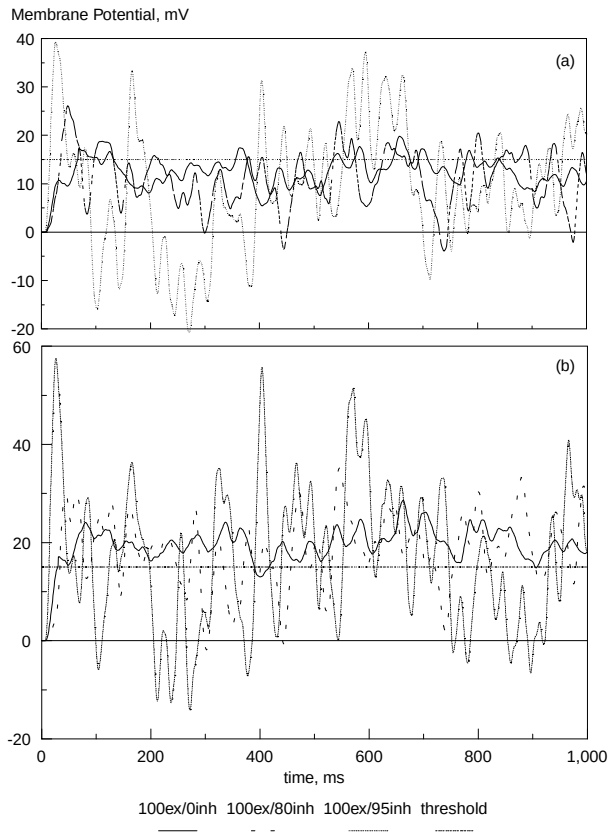

Fig. 3: Membrane Potential without and with inhibition for the cases **100ex/0inh**, **100ex/80inh** and **100ex/95inh**) with the same Mean Input Current (I_{M_i}): (a) I_{M_i} = 80pA, (b) I_{M_i} = 130pA. Higher input frequencies are required to obtain the same I_{M_i} for the cases with inhibition. This results to a higher excitatory component of Mean Input Current which shifts the mean fluctuation level of the Membrane Potential above 0mV.

inhibition is increased, we took two snapshots of the membrane potential for I_{M_i} = 80pA and I_{M_i} = 130pA (vertical lines on Fig. 2), for the cases of 100ex/0inh, 100ex/80inh and 100ex/95inh. These are shown in Fig. 3 from 0ms to 1000ms. As it can be observed, inhibition increases frequency of the fluctuations of the membrane potential and this can be proved by looking at the periodograms (plots of power *vs* frequency where power is defined as the magnitude of the Fourier Transform squared, of the membrane potential) of the snapshots (Fig. 4), which give the frequency density of the average power of the membrane potential (Haykin, 1995). From the periodograms we can see that with inhibition (Figs. 4b, 4d) we get more significant variations in terms of amplitude in the entire frequency range, indicating the presence of more frequency components and thus more fluctuations (i.e., fluctuations of increased frequency) in the membrane potential. It has to be noted that the increased fluctuations do not change the mean saturation level of the membrane potential. This is because of the higher excitatory input current which had to be induced when the number of inhibitory inputs was increased, in order to obtain the same mean input current I_{M_i} (see Fig. 2). In addition, the amplitude of the membrane potential fluctuations increases with inhibition as it can be seen from Fig. 5. This shows that the histogram distributions of the membrane potential widen with inhibition indicating that the membrane potential hits more times lower and higher amplitudes. Therefore, in the case of low I_{M_i} (e.g., 80pA, Fig. 3a), where the mean saturation level of the membrane potential is below the threshold, the membrane potential of the 100ex/80inh and the 100ex/95inh cases is able to exceed the threshold more frequently than in the 100ex/0inh case due to the greater amplitude fluctuations and thus give a higher output frequency. However, in the case of high I_{M_i} (e.g., 130pA, Fig. 3b) the mean saturation level of the membrane potential is above the threshold and so in the 100ex/80inh and the 100ex/95inh cases, due to the high amplitude fluctuations again, the membrane potential is able to go below the threshold more frequently than in the 100ex/0inh case and thus give a lower output frequency. This explains the reduced slope of the sigmoidal characteristic curves of Fig. 2 in the presence of inhibition. Alternatively, this can be also explained intuitively as follows: the total PSR at any given time is the sum of the excitatory and inhibitory PSRs occurring within a certain window. Thus the distribution of the total PSR will be the difference between the two binomial distributions (ignoring the ramped edges of the PSR). Adding more inhibition, requires more excitation to achieve the same mean. However, the variance of the distribution widens (as shown in Fig. 5). When subtracting two independent distributions, the means subtract while the variances add. This point has previously been mentioned by Amit & Brunel (1997) (where they showed that spontaneous

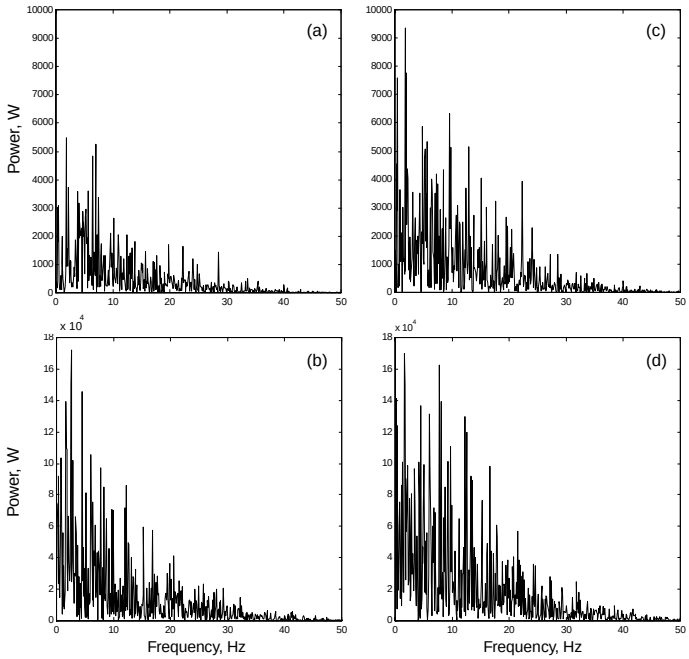

Fig. 4: Periodograms of the Membrane Potential with and without inhibition with the same Mean Input Current (I_{M_i}): (a) I_{M_i} = 80pA, 100ex/0inh, (b) I_{M_i} = 80pA, 100ex/95inh, (c) I_{M_i} = 130pA, 100ex/0inh, (d) I_{M_i} = 130pA, 100ex/95inh. Notice the differences in the Power scale.

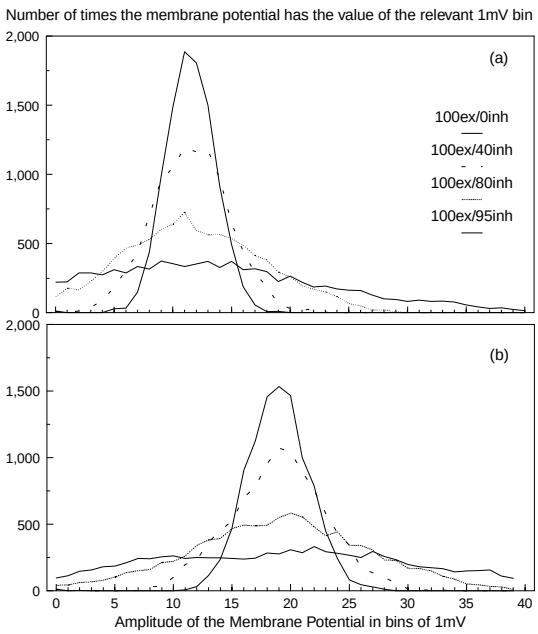

Fig. 5: Histogram distributions of the Membrane Potential without inhibition and for three cases with inhibition (**100ex/0inh**, **100ex/40inh**, **100ex/80inh and 100ex/95inh**) with the same Mean Input Current (I_{M_i}): (a) I_{M_i} = 80pA, (b) I_{M_i} = 130pA.

activity becomes self-stabilising in the presence of inhibition), but it has not been rigorously proved as it is done here.

The other important point that can be deduced from Fig. 2 is that the decrease of the slope of the sigmoid output characteristic, which denotes the gain of the transfer function, seems to be proportional to the number of inhibitory inputs present. The gain is best reduced when the number of inhibitory inputs becomes nearly the same as the number of excitatory inputs (100ex/95inh case). At first glance this is biologically unrealistic since there is physiological evidence that inhibitory synapses constitute approximately 15% of the synapses on cortical neurons (Peters, 1987). However, inhibitory synapses in real cells are concentrated proximally to the soma (Peters, 1987; Gu *et al*., 1993) and have relatively large conductances and long durations (Douglas & Martin, 1991), suggesting that the impact of IPSPs on the membrane potential is greater than the 15%. In addition, inhibitory neurons tend to fire at higher rates (Connors & Gutnik, 1990). Hence, it is reasonable to consider, like we did, that there is a high level of inhibition. Therefore, inhibition can be considered as another means of controlling the gain of the transfer function of the neuron (for gain control through partial somatic reset, see (Bugmann *et al*., 1997). The gain control mechanism by inhibition, is not shown or implied in the work of Amit and Brunel (1997).

Shadlen and Newsome (1994; 1998) introduced the possibility of a balanced excitation and inhibition and incorporated it in their model in order to explain irregular cortical neural firing (something also explored in Feng & Brown 1998). Tsodyks and Sejnowski (1995) also used balanced recurrent excitation with feedback inhibition, in combination with other mechanisms, in a network of integrate and fire neurons, for obtaining high firing variability. Van Vreeswiijk and Sompolinsky (1996; 1998) demonstrated that chaotic dynamics can be produced when there is a balance between excitation and inhibition. However, none of these authors showed how the firing rate can be controlled in such a case. When there is a balance of excitation and inhibition the mean input current is zero (see Fig. 2) and the neuron is firing due to the fluctuations. The relationship of the input frequency (f_j) and the firing rate of the neuron for the balanced case of 100 excitatory inputs and 100 inhibitory inputs (100ex/100inh, Fig. 6) gives a bell-shape curve. This indicates that the frequency and the amplitude of the membrane potential fluctuations have small values at low input frequencies, they peak at input frequencies of around $f_j \simeq 500$Hz (which is probably the maximum firing rate of cortical neurons) and then reduce again as we approach input frequencies of $f_j \simeq 1000$Hz. This is indicated by the membrane potential snapshots at f_j = 100Hz, 500Hz and 900Hz from 0 to 1000ms, shown in Fig. 7. Therefore, we can deduce that in the case of balanced excitation and inhibition (where the neuron is explicitly firing due to the fluctuations), the firing rate can be controlled by the level of the mean input frequency.

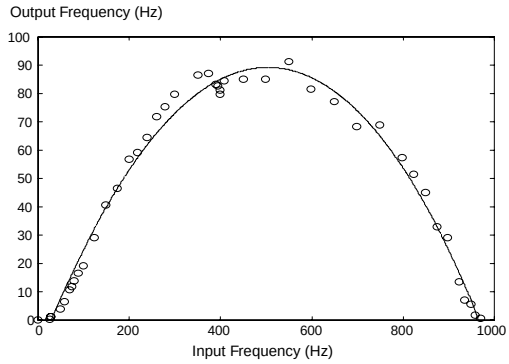

Fig. 6: Mean Input Frequency (f_j) *vs* Firing Rate, for the case of balanced excitation and inhibition (100ex/100inh).

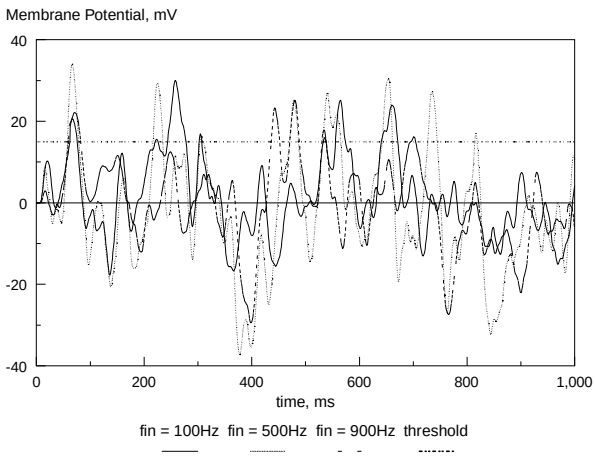

Fig. 7: Membrane Potential for the balanced case of excitation and inhibition, **100ex/100inh**, for three different values of mean input frequency f_j = 100Hz, 500Hz and 900Hz.

Concluding, in this paper we showed that the introduction of inhibition, not only reduces the mean input current for the same mean input frequency (shifting the transfer function), but it also decreases the slope of the transfer function (gain) of the neuron. The effect on the slope is due to increasing (i) the frequency of the fluctuations and (ii) the amplitude of the fluctuations of the membrane potential (at a given level of mean input current) around its mean saturation value. This goes beyond the assumption underlying the formal neuron used in Artificial Neural Networks where it is assumed that positive and negative inputs add linearly and then pass through a fixed sigmoidal transfer function, whereas in the TNLI the sigmoidal transfer function is modified by the signals passing through it. In other

words, with inhibition, weak signals need less amplification to produce the same level of output frequency but strong signals need more amplification. These results also demonstrate that the TNLI, despite its simplicity, can give an insight on certain phenomena that are not easily revealed by experimental studies. In addition, it has been shown that inhibition can be used for controlling the gain of the transfer function of the neuron, with the gain being a decreasing function of the number of inhibitory inputs. Finally, we demonstrated that in the case of balanced excitation and inhibition, when the neuron is totally driven by membrane potential fluctuations, the firing rate can be controlled by the level of the mean input frequency. Elsewhere (Christodoulou & Bugmann, 1999a; b) we examine the effect of inhibition in the neuronal firing variability.

References

Amit, D. J., & Brunel, N, 1997. *Cerebral Cortex*, **7**, 237-252.

Bressloff, P. C. & Taylor, J. G. 1991. *Neural Networks*, **4**, 789-801.

Bugmann, G. 1992. *Biol. Cyber.*, **68**, 87-92.

Bugmann, G., Christodoulou C. & Taylor, J. G. 1997. *Neural Computation*, **9**, 5, 985-1000.

Burke, R. E. & Rudomin, P. 1977 In *Handbook of Physiology, The nervous system*, Section 1, Vol. 1, Part 2, Chapter 24, (ed. E. R. Kandel), American Physiological Society, Bethesda, Maryland, USA, 877-944.

Christodoulou, C., Bugmann, G., Taylor, J. G. & Clarkson, T. G. 1992. *Proc. of the Int. Joint Conf. on Neural Networks*, Beijing, **III**, 165-170.

Christodoulou, C., Clarkson T. G., Bugmann, G & Taylor J. G. 1994. *Proc. of the IEEE Int. Conf. on Neural Networks (ICNN '94)*, Orlando, Florida, USA, **IV**, 2239-2244.

Christodoulou, C. & Bugmann, G. 1999a . *Proc of the Int. Workshop on Neuronal Coding (NCWS '99)*, Osaka, Japan, 41-44.

Christodoulou, C. & Bugmann, 1999b. Submitted to *Biosystems* (Special Issue on Neuronal Coding), Dec. 1999.

Clarkson, T. G., Ng, C. K., Gorse, D & Taylor, J. G. 1992 . *IEEE Trans. on Computers*, **41** (12), 1552-1561.

Connors, B. W. & Gutnick, M. J. 1990. *Trends in Neurosciences*, **13** (3), 99-104.

Douglas, R. & Martin K. 1991. *J. of Physiol. (London)*, **440**, 735-769.

Feng, J. & Brown, D. 1998. *Biol. Cybern.*, **78**, 369-376.

Gu, Q., Prezvelazquez, J., Angelides, K. & Cynader, M. 1993. *J. Comp. Neurol.*, **333**, 94-108.

Haykin, S. 1995 *Communication Systems* (3rd ed), Canada: John Wiley, ch. 4, 252-264.

Hodgkin, A. L. & Huxley, A F. 1952. *J. of Physiol.* (London), **117**, 500-544.

Küpfmüller, K. & Jenik, F. 1961. *Kybernetik*, Band I, Heft 1, 1-6.

Lapique, L. 1907. *J. Physiol. Pathol. Gen.*, **9**, 620-635.

McCulloch, W. S. and Pitts, W. 1943. *Bull. Math. Biophys.*, **5**, 115-133.

Nicholls, J. G., Martin, A. R. & B. G. Wallace, B. G. 1992 *From Neuron to Brain: A Cellular and Molecular Approach to the Function of the Nervous System*, Sunderland, MA, USA, Sinauer Associates.

Peters, A. 1987. In *Synaptic Function*, (ed. G. Edelman, W. Gall & W. Cowan) New York, Wiley, 373-397.

Rall, W. 1964. *In: Neural Theory and Modelling*. (ed. Reiss,. R. F.) Stanford, Stanford University Press, 73-77.

Rumelhart, D. E., Hinton, G. E. & Williams 1986. *Nature*, **323**, 533-536.

Shadlen, M. N. & Newsome, W. T. 1994. *Curr. Opin. Neurobiol.*, **4**, 569-579.

Shadlen, M. N. & Newsome, W. T. 1998. *J of Neurosci.*, **18**, 3870-3896.

Shepherd, G. M. & Koch, C. 1990 Appendix: Dendritic Electrotonus and Synaptic Integration. *The Synaptic Organisation of the Brain*, (3rd ed.), (ed. Shepherd, G. M.) Oxford Univ Press.

Tsodyks, M. V. & Sejnowski, T., 1995. *Network: Computation in Neural Systems*, **6**, 111-124.

Van Vreeswijk, C. & Sompolinsky, H. 1996. *Science*, **274**, 1724-1726.

Van Vreeswijk, C. & Sompolinsky, H. 1998. *Neural Computation*, **10**, 1321-1371.

Walmsley, B. and Stuklis, R. 1989. *J. of Neurophysiol.*, **61**, 681-687.